electronics

MDPI

Article

Fault Diagnosis of Gas Insulated Switchgear Isolation Switch Based on Improved Support Vector Data Description Method

Nan Zhang [1,*], Tianchi Wu [1], Yunpeng Zhang [1], Bo Yin [1], Xuebin Yang [1], Chengliang Liu [2] and Senxiang Lu [2]

[1] State Grid Liaoning Extra High Voltage Company, Shenyang 110003, China; wtc_jx@ln.sgcc.com.cn (T.W.); zyp_jx@ln.sgcc.com.cn (Y.Z.); yb1_jx@ln.sgcc.com.cn (B.Y.); yxb_jx@ln.sgcc.com.cn (X.Y.)
[2] College of Information Science and Engineering, Northeastern University, Shenyang 110003, China; 2370754@stu.neu.edu.cn (C.L.); lusenxiang@ise.neu.edu.cn (S.L.)
* Correspondence: zn2_jx@ln.sgcc.com.cn

Abstract: To improve the efficiency and precision of fault diagnosis for isolation switches within Gas-insulated switchgear (GIS), this study introduces an advanced technique utilizing an enhanced support vector data description (SVDD) algorithm. Initially, various operational states of the GIS isolation switch are simulated, and the corresponding vibration signals are captured. Subsequently, both the entropy and time-domain features of these signals are extracted to construct a multi-dimensional feature space. High-dimensional feature datasets are then reduced in dimensionality using the kernel principal component analysis (KPCA) method. Furthermore, the conventional SVDD algorithm is modified by incorporating a penalty factor, which allows for a more adaptable classification boundary. This adaptation not only focuses on positive samples but also considers the influence of selected negative samples on the classification hypersphere. Finally, the collected experimental data are classified and predicted. The results indicate that this GIS fault-diagnosis approach effectively overcomes the limitations of traditional methods, which are heavily dependent on training sample data and demonstrate poor algorithm generalization performance. This method is proven to be applicable for the fault diagnosis of isolation switches in GIS.

Keywords: isolation switch in GIS; vibration signal; improved SVDD; KPCA; fault diagnosis

check for updates

Academic Editor: Ahmed Abu-Siada

Received: 4 January 2025
Revised: 22 January 2025
Accepted: 26 January 2025
Published: 29 January 2025

Citation: Zhang, N.; Wu, T.; Zhang, Y.; Yin, B.; Yang, X.; Liu, C.; Lu, S. Fault Diagnosis of Gas Insulated Switchgear Isolation Switch Based on Improved Support Vector Data Description Method. *Electronics* **2025**, *14*, 540. https://doi.org/10.3390/electronics14030540

Copyright: © 2025 by the authors. Licensee MDPI, Basel, Switzerland. This article is an open access article distributed under the terms and conditions of the Creative Commons Attribution (CC BY) license (https://creativecommons.org/licenses/by/4.0/).

1. Introduction

Gas-insulated switchgear (GIS) plays a crucial role in power systems by ensuring the control and protection of high-voltage power grids [1,2]. Isolation switches within the GIS are primarily exposed to two types of faults, mechanical faults and electrical discharge faults. Mechanical faults are the more common type, accounting for 73% of all faults, and the main problems include jamming of the operating mechanism, loosening of the trans-mission mechanism, and incomplete opening and closing actions. Currently, most of the maintenance of isolation switchgear adopts a strategy based on its operating condition [3–5]. Nevertheless, the domestic research on the fault-diagnosis technology of the isolation switch is still insufficient. To guarantee the stability and safety of the entire power system, it is necessary to conduct real-time condition monitoring and fault diagnosis of the isolation switch in GIS.

The mechanical vibration signals generated when an isolation switch is opened and closed contain crucial information about the equipment's condition. We can achieve the effective fault diagnosis of isolation switches in GIS by collecting vibration signals, extracting critical signal features, and using machine learning techniques to evaluate the

equipment's condition. For example, Li C et al. developed a mechanical defect identification model using the correlation coefficient method and multilayer classifiers by simulating the vibration generated by the poor contact and loose bracket of GIS isolation switches [6]. Janssens O et al. designed the support vector machine model optimized with a combination of S-transform and particle swarm algorithms for identifying mechanical defects in GIS equipment [7]. Yue Y et al. proposed a GIS disconnector fault-diagnosis method based on FA-SVM, which can effectively identify two common faults: jamming and looseness [8]. Zhang J et al. designed an intelligent system for detecting the mechanical characteristics of GIS disconnectors, employing a fault-diagnosis method for GIS disconnectors based on the White Shark Optimization Algorithm. This work provides a theoretical basis for the research on key technologies of digital sensing and fault early warning for disconnectors in GIS [9]. Presently, the majority of research on the mechanical vibration of GIS equipment is centered around basic defect simulation or on-site detection, and there is still a comparative shortage of in-depth discussions on the nonlinear characteristics of the mechanical vibration of GIS isolation switches [10]. Moreover, an abundance of features during fault feature extraction and selection can heighten the analysis complexity, while conventional population intelligence algorithms, like particle swarm optimization, may face challenges, such as extended iteration periods, susceptibility to local optima, and inadequate model robustness during support vector machine optimization.

In order to compensate for the shortcomings of the existing research in practical applications, this paper builds a multidimensional feature space by monitoring the vibration signals of the isolation switches in GIS during their opening and closing and extracting their entropy and time-domain features. Then, the kernel principal component analysis (KPCA) algorithm is used to downscale the features and select the main components according to the cumulative contribution rate. Ultimately, a fault-diagnosis model incorporating enhancements to the support vector data description (SVDD) algorithm is developed. The model modifies the classification interface by adding a penalty factor to the imbalanced positive and negative samples, enabling the identification of different operating states of the isolation switch, thus compensating for the deficiencies of existing methods in practical applications. In the future, some fault-tolerant and data-driven algorithms are expected to be incorporated into the GIS disconnector fault diagnosis, enhancing diagnostic performance [11,12].

2. Vibration Signal Acquisition and Feature Extraction

In this study, the isolation switch manufactured by an electrical equipment manufacturing company located in Shenyang is used as the object of study. The mechanical vibration generated by this disconnect switch during operation can be characterized by determining the acceleration at specific measurement points. The vibration signal acquisition system comprises three key components an acceleration sensor, an NI data acquisition card, and a computer console. The IEPE piezoelectric acceleration sensor, model CT1010LF, is used in this study, as shown in Figure 1a, which has a measurement capability of up to 50 g and a wide frequency response range, as well as high sensitivity characteristics, and can be fixed directly to the device under test, eliminating the need to disassemble the casing and facilitating the measurement. The NI9250 acquisition card is equipped with an IEPE excitation source, which is connected to the computer console through 2 mA. The NI9250 acquisition card is equipped with an IEPE excitation source that powers a piezoelectric transducer through a 2 mA constant current source and captures its output acceleration signal in meters per second squared. The console-mounted DAQ Express software 5.0 is responsible for driving the data acquisition card, as well as the storing and processing

the acquired data. Figure 1b–d show the accelerometer mounting location, the physical acquisition device, and the acquisition software interface, respectively.

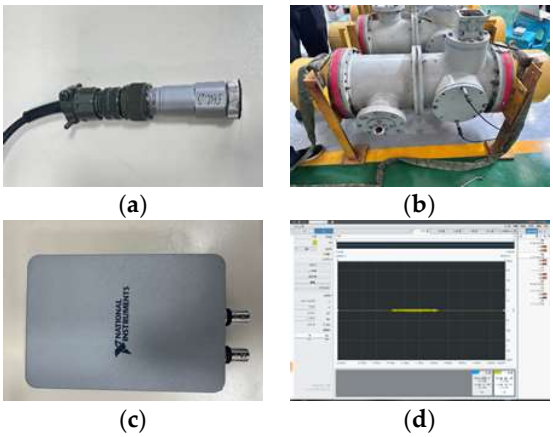


Figure 1. (**a**) IEPE piezoelectric acceleration sensor; (**b**) accelerometer mounting location; (**c**) physical acquisition device; (**d**) acquisition software interface.

Through experimental examination and a signal comparison, the sampling frequency determined in this study is 10,000 times per second, with a total of 15,000 data points sampled. The study mainly simulates four typical operation scenarios of the isolation switch, covering the normal operation of the isolation switch and several fault situations. The fault conditions include the operating mechanism stuck, the single-phase connecting rod off, and two-phase connecting rod off.

The vibration signals from the GIS isolation switches in the GIS present highly non-constant characteristics, and such signals can be regarded as a nonlinear time series. The concept of information entropy was originally introduced by Shannon to assess the non-constant nature of the time series and their complexity [13]. By calculating the entropy of a vibration signal, it is possible to reveal the uncertainty of the signal and thus characterize the fault-related features.

In this research, we utilize the information entropy theory to derive eight distinct entropy metrics from vibration signals as feature parameters. These include power spectrum entropy, singular spectrum entropy, energy entropy, approximation entropy, sample entropy, fuzzy entropy, alignment entropy, and envelope entropy. Following the completion of entropy feature extraction from the vibration signal, we combine these entropy features with the time domain features to create a feature matrix, aiming to build a comprehensive feature set. These time-domain features are global metrics used to quantify the differences in waveforms over the entire sequence of signals, and they complement the local features of entropy in order to more comprehensively differentiate between different fault signal waveforms. The time-domain features that were chosen comprise variance, cliff, skewness, root mean square, square root magnitude, waveform factor, peak factor, pulse factor, and margin factor.

After generating inputs with multidimensional features, this study applies KPCA to decrease the data's dimensionality. This process simplifies the data structure while removing redundant information from the data with the aim of retaining the key elements in the dataset. KPCA can be considered as a non-linear enhancement of the conventional principal component analysis (PCA) technique, wherein it conducts PCA on the data within a high-dimensional feature space by initially converting the original data to this space via a non-linear transformation [14,15]. The kernel function plays a key role in KPCA, which skillfully converts the complex dot product computation in the high-dimensional space into kernel operations in the original space to realize non-linear feature extraction. If the

variance contribution ratio of the top few principal components in the feature space reaches a certain predetermined threshold, these principal components are chosen to represent the original data.

3. Fault Diagnosis Model of the ISOLATION Switch Based on Improved SVDD

3.1. SVDD Algorithm Principle

The SVDD algorithm is a well-established single-class classification algorithm that originated from the traditional SVM. It differs mainly from the traditional SVM in that the SVDD specializes in small-sample datasets and handles non-linear data efficiently [16]. The SVDD is an individual classification algorithm that has been specifically tailored to handle imbalanced datasets. The core of the algorithm is to determine a minimum enclosing sphere in the feature space that encompasses all of the training sample points [17]. This sphere is centered at point a and has a radius of R. Sample points inside the sphere are classified into positive classes, while samples outside the sphere are not classified with those inside. The SVDD algorithm aims to identify the distinctive hypersphere by reducing its radius. When training the model, the SVDD does not need to rely on other classes of data samples and is well suited for classification and recognition problems with unbalanced datasets. Next, the article describes the mathematics of the SVDD algorithm.

The simplest mathematical model of the SVDD algorithm is given by the following:

$$\min_{R,a} R^2, (x_i - a)^{\mathrm{T}}(x_i - a) \leq R^2,\ i = 1, 2, \cdots, N_T \tag{1}$$

where R represents the radius of the hypersphere, a is the center of the hypersphere, and N_T is the number of training samples, and it maps the training samples into a high-dimensional feature space. The Lagrangian function constructed for this optimization problem is given by the following:

$$L(R, a, \lambda_i) = R^2 + \sum_{i=1}^{N_T} \lambda_i \left(\mathbf{x}_i^2 - 2ax_i + a^2 - R^2 \right),\ \lambda_i \geq 0 \tag{2}$$

Through the application of Karush–Kuhn–Tucker (KKT) conditions, the following complementary slackness conditions are derived:

$$\lambda_i \left(\mathbf{x}_i^2 - 2ax_i + a^2 - R^2 \right) = 0 \tag{3}$$

If $\lambda_i = 0$, $\mathbf{x}_i^2 - 2ax_i + a^2 - R^2 \neq 0$ or if $\mathbf{x}_i^2 - 2ax_i + a^2 - R^2 = 0$, $\lambda_i \neq 0$.

The condition of stationarity requires that the gradient of the Lagrange function with respect to the original variables is zero. Establishing the stationarity condition leads to the following:

$$\begin{aligned} \frac{\partial L(a, R, \lambda_i)}{\partial a} &= -2 \sum_{i=1}^{N_T} \lambda_i \boldsymbol{x}_i + 2 \sum_{i=1}^{N_T} \lambda_i \boldsymbol{a} = 0 \\ \frac{\partial L(a, R, \lambda_i)}{\partial R} &= 2R - 2R \sum_{i=1}^{N} \lambda_i = 0 \end{aligned} \tag{4}$$

Further simplification yields the following:

$$\boldsymbol{a} = \frac{\sum_{i=1}^{N_T} \lambda_i x_i}{\sum_{}^{N_T} \lambda_i} = \sum_{i=1}^{N_T} \lambda_i \boldsymbol{x_i} \tag{5}$$

The complementary slackness conditions for the SVDD algorithm are as follows:

$$\lambda_i\left(x_i^2 - 2ax_i + a^2 - R^2\right) = 0,\ i = 1, 2, \cdots, N_T \tag{6}$$

$$\begin{aligned} L(a, R, \lambda_i) &= R^2 + \sum_{i=1}^{N_T} \lambda_i x_i^2 - 2\sum_{i=1}^{N_T} \lambda_i x_i a + \sum_{i=1}^{N_T} \lambda_i a^2 - \sum_{i=1}^{N_T} \lambda_i R^2 \\ &= \sum_{i=1}^{N_T} \lambda_i x_i^2 - 2\sum_{i=1}^{N_T} \lambda_i x_i a + a^2 = \sum_{i=1}^{N_T} \lambda_i x_i^2 - 2aa + a^2 = \sum_{i=1}^{N_T} \lambda_i x_i^2 - a^2 \\ &= \sum_{i=1}^{N_T} \lambda_i(\boldsymbol{x_i}, \boldsymbol{x_i}) - \sum_{i,j=1}^{N_T} \lambda_i \lambda_j(\boldsymbol{x_i}, \boldsymbol{x_j}) \end{aligned} \tag{7}$$

Based on the transformation outlined above, the dual problem is obtained:

$$\max_{\lambda}\left\{\sum_{i=1}^{N} \lambda_i(\boldsymbol{x_i}, \boldsymbol{x_i}) - \sum_{i,j=1}^{N} \lambda_i \lambda_j(\boldsymbol{x_i}, \boldsymbol{x_j})\right\} \tag{8}$$

Subject to the following:

$$\sum_{i=1}^{N_T} \lambda_i = 1 \tag{9}$$

where $\lambda_i \geq 0, \mathrm{i} = 1, 2, \cdots, N_T$.

By solving the numerical values from the above formulas, the SVDD algorithm determines the radius and center of the classification hypersphere:

$$a = \sum_{i=1}^{N_T} \lambda_i \boldsymbol{x_i} \tag{10}$$

$$\begin{aligned} R^2 &= \frac{1}{N_b}\sum_{k=1}^{N_b}\left\{x_k - a^2\right\} = \frac{1}{N_b}\sum_{k=1}^{N_b}\left\{x_k - \sum_{i=1}^{N_T} \lambda_i x_i^2\right\} \\ &= \frac{1}{N_b}\sum_{k=1}^{N_b}\left\{x_k \cdot x_k - 2\sum_{i=1}^{N_T} \lambda_i x_i \cdot x_k + \sum_{i,j=1}^{N_T} \lambda_i \lambda_j x_i x_j\right\} \end{aligned} \tag{11}$$

$\varphi(x)$ is obtained by mapping the training and testing samples into a high-dimensional feature space using a mapping function. The formula for the radius of the hypersphere is given by the following:

$$R^2 = \frac{1}{N_b}\sum_{s=1}^{N_b}\left\{\begin{array}{l} \varphi(\boldsymbol{x}_s)\cdot\varphi(\boldsymbol{x_s}) - 2\sum_{i=1}^{N} \lambda_i \varphi(\boldsymbol{x}_s)\cdot\varphi(\boldsymbol{x_i}) + \\ \sum_{i,j=1}^{N} \lambda_i \lambda_j \varphi(\boldsymbol{x_i})\cdot\varphi(\boldsymbol{x_j}) \end{array}\right\} \tag{12}$$

After transforming through the Gaussian kernel function $Kernel(\boldsymbol{x_i}, \boldsymbol{x_j}) = \boldsymbol{x_i}\cdot\boldsymbol{x_j}$ and considering the use of the classical Gaussian kernel function in this algorithm, the following expression is derived:

$$Kernel(\boldsymbol{x_i}, \boldsymbol{x_j}) = \boldsymbol{x_i}\cdot\boldsymbol{x_j} = k(\boldsymbol{x_i}, \boldsymbol{x_j}) = \exp\left(-\frac{\boldsymbol{x_i} - \boldsymbol{x_j}^2}{2\sigma^2}\right) \tag{13}$$

In the above expression, $K(\boldsymbol{x_i}, \boldsymbol{x_i}) = \exp\left(-\frac{\boldsymbol{x_i}-\boldsymbol{x_i}^2}{2\sigma^2}\right) = 1$ can be further derived as follows:

$$\begin{aligned} R^2 &= \frac{1}{N_b}\sum_{s=1}^{N_b}\left\{\begin{array}{l} k(x_s, \boldsymbol{x}_s) - 2\sum\limits_{i=1}^{N}\lambda_i k(x_s, \boldsymbol{x_i}) + \\ \sum\limits_{i,j=1}^{N}\lambda_i\lambda_j k\left(\boldsymbol{x_i}, \boldsymbol{x_j}\right) \end{array}\right\} \\ &= 1 + \sum_{i,j=1}^{N}\lambda_i\lambda_j k\left(\boldsymbol{x_i}, \boldsymbol{x_j}\right) - 2\frac{1}{N_b}\sum_{k=1}^{N_b}\sum_{i=1}^{N}\lambda_i k(\boldsymbol{x_s}, \boldsymbol{x_i}) \end{aligned} \tag{14}$$

where N_b represents the total number of samples in the classification interface, x_s is the number of support vectors in the classification interface, $K\left(\boldsymbol{x_i}, \boldsymbol{x_j}\right)$, $K(\boldsymbol{x_s}, \boldsymbol{x_i})$ denotes the Gaussian kernel function, and λ_i, λ_j is the Lagrange multiplier. Where $i, j = 1, 2, \cdots, N_T$.

During the process of maximizing the gap between two margin interfaces, based on the dual complementary slackness conditions in the KKT conditions, the following formula $\lambda_i\left(x_i^2 - 2ax_i + a^2 - R^2\right) = 0,\ i = 1, 2, \cdots, N$ is derived. If $\lambda_i > 0$ holds, then $\left[x_i^2 - 2ax_i + a^2 - R^2\right] = 0$ is obtained. This signifies that the sample is a positive class sample, and α represents the support vector on the classification interface. Otherwise, if $\lambda_i = 0$, then $\left[x_i^2 - 2ax_i + a^2 - R^2\right] < 0$ holds, indicating that the sample is a positive class sample within the inclusive range of the hypersphere classification interface.

For a new test sample $\boldsymbol{x}'$, the decision function is constructed for classification. Utilizing the Gaussian kernel function, the decision function is expressed as follows:

$$\begin{aligned} &\varphi(x') - \sum_{i=1}^{N}\lambda_i\varphi(x_i)^2 = \varphi(x')\cdot\varphi(x') - \\ &2\sum_{i=1}^{N}\lambda_i\varphi(x')\cdot\varphi(x_i) + \sum_{i,j=1}^{N}\lambda_i\lambda_j\varphi(x_i)\cdot\varphi(x_j) \end{aligned} \tag{15}$$

After transformation through the Gaussian kernel function $Kernel\left(\boldsymbol{x_i}, \boldsymbol{x_j}\right) = \varphi(\boldsymbol{x_i})\cdot\varphi\left(\boldsymbol{x_j}\right)$, the expression becomes the following:

$$Kernel\left(x_i, x_j\right) = k\left(x_i, x_j\right) = \varphi(x_i)\cdot\varphi\left(x_j\right) = \exp\left(-\gamma||x_i - x_j||^2\right) \tag{16}$$

In the above formula, $K(x', x_i) = \exp\left(-\gamma||x' - x_i||^2\right) = 1$, according to this derivation, the following can be obtained:

$$\begin{aligned} &\varphi(x') - \sum_{i=1}^{N}\lambda_i\varphi(x_i)^2 = 1 - 2\sum_{i=1}^{N}\lambda_i k(x', x_i) + \\ &\sum_{i,j=1}^{N}\lambda_i\lambda_j k\left(x_i, x_j\right) \end{aligned} \tag{17}$$

In this formula, if $1 - 2\sum\limits_{i=1}^{N}\lambda_i k(\boldsymbol{x}', \boldsymbol{x}_i) + \sum\limits_{i,j=1}^{N}\lambda_i\lambda_j k\left(\boldsymbol{x_i}, \boldsymbol{x_j}\right) > R^2$, which indicates that the test sample $\boldsymbol{x}'$ is an anomalous fault class sample. If the formula $1 - 2\sum\limits_{i=1}^{N}\lambda_i k(\boldsymbol{x}', \boldsymbol{x}_i) + \sum\limits_{i,j=1}^{N}\lambda_i\lambda_j k\left(\boldsymbol{x_i}, \boldsymbol{x_j}\right) \leq R^2$, it suggests that the test sample $\boldsymbol{x}'$ is a normal sample. When the Gaussian kernel parameter value γ is large, the width of the Gaussian function is narrow, which means that only samples that are very close to each other will be considered similar. This may lead to the algorithm overfitting the training data, as it will attempt to precisely include each training sample within the hypersphere, including potential noise and outliers. This will reduce the algorithm's generalization ability based on unseen data, resulting in a decrease in test accuracy. When the Gaussian kernel parameter γ is small, the width of the Gaussian function is wide, which means that samples that are farther apart will

also be considered similar. This may cause the algorithm to fail to capture the structure of the data well, as it might include samples that should not be part of the hypersphere. The result could be an excessively large hypersphere that fails to effectively distinguish between normal and abnormal data, thus reducing the detection accuracy.

3.2. Improved SVDD Algorithm

The traditional SVDD algorithm only relies on a single positive class sample for sample data training and does not require the participation of other samples. However, because the traditional SVDD algorithm only considers one type of sample data in the classification, the classification decision interface obtained after classification optimization is often close to the positive class sample. Since the goal of SVDD is to minimize the hyper-sphere that contains all the positive class sample, the resulting decision boundary is very close to the normal sample. This means that any slight anomaly may lead to misjudgment, thereby reducing the generalization ability; at the same time, if the training set is mixed with other samples, the SVDD algorithm may expand the hyper-sphere to include these anomalies, resulting in an overly loose decision boundary, which will affect the generalization performance of the algorithm. This, in turn, can lead to the ineffectiveness of the algorithm's fault-detection model as a classifier [18,19]. Therefore, the traditional SVDD algorithm has certain limitations as a fault-diagnosis classifier for the isolation switch in GIS.

This article suggests enhancing the SVDD algorithm, which can effectively address the issue that the classification interface deviation of the SVDD algorithm is not high due to only considering the positive class samples, resulting in the low generalization performance of the algorithm and the insufficient detection accuracy. The design concept of the improved SVDD algorithm can be summarized as follows: based on the SVDD algorithm, the method of adding penalty factors to both types of samples in the training dataset is employed, enabling the algorithm to take into account all samples. This will cause the classification interface to shift towards the side of the negative class samples, increase the generalization performance of the algorithm, and subsequently improve the detection accuracy of the model. The following will introduce the mathematical mechanism of improving the SVDD algorithm based on the mathematical mechanism of the SVDD algorithm. The penalty factor is added to the positive and negative samples of the traditional SVDD algorithm, and the mathematical model expression is obtained:

$$F(R, a, \xi_l, \xi_m) = \min\left(R^2 + C_1 \sum_{i=1}^{n} \xi_l + C_2 \sum_{i=1}^{n} \xi_m\right) \tag{18}$$

The constraints on the above model expression are as follows:

$$(x_l - a)^T (x_l - a) \leq R^2 + \xi_l, \xi_l \geq 0, \ \forall l = 1, 2, \cdots, n \tag{19}$$

$$(x_m - a)^T (x_m - a) > R^2 + \xi_m, \xi_m \geq 0, \ \forall m = 1, 2, \cdots, n \tag{20}$$

In the above formula, R represents the spherical radius of the classification interface; a represents the center of the sphere of the classified hypersphere; C_1 and C_2 represent the introduced penalty constants, which control the size of the loss function between normal and negative samples. ξ_l and ξ_m are the penalty factors, which are used to regulate the distance between positive and negative samples, adjust the position of the classification interface, and enhance the generalization performance of the algorithm. This is a key improvement over the traditional SVDD algorithm.

The Lagrangian function is introduced, and the partial derivative is obtained by substituting the result into the original function to derive the dual function. The dataset

of the training sample is mapped to a high-dimensional feature space using the Gaussian kernel function, resulting in a transformed original function.

$$\begin{aligned} L = \max & \sum_{l=1}^{n} \alpha_l K(\boldsymbol{x_l} \cdot \boldsymbol{x_l}) - \sum_{m=1}^{n} \alpha_m K(\boldsymbol{x_m} \cdot \boldsymbol{x_m}) \\ & - \sum_{l=1,i=1}^{n} \alpha_l \alpha_i K(\boldsymbol{x_l} \cdot \boldsymbol{x_i}) + 2 \sum_{m=1,j=1}^{n} \alpha_m \alpha_j K(\boldsymbol{x_m} \cdot \boldsymbol{x_j}) \\ & - \sum_{m=1,k=1}^{n} \alpha_m \alpha_k K(\boldsymbol{x_m} \cdot \boldsymbol{x_k}) \end{aligned} \tag{21}$$

Equation (22) can be regarded as the solution of a convex quadratic programming problem, and the spherical center can be obtained by solving it:

$$a = \sum_{l=1}^{n} \alpha_l \phi(\boldsymbol{x}_l) - \sum_{m=1}^{n} \alpha_m \phi(\boldsymbol{x}_m) \tag{22}$$

As can be seen from the above formula, the improved SVDD algorithm can take into account the entire data sample. The inclusion of a penalty factor brings the algorithm's classification interface closer to a balance between the two sample types, enhancing the algorithm's classification performance and remarkably boosting the accuracy of detecting minority samples.

4. Analyzing and Validating Isolation Switch Fault Diagnosis in GIS Through Experiments

4.1. Data Dimensionality Reduction Based on KPCA

KPCA can calculate the components that are strongly related to the original signal, reduce the data, and remove its redundant information. After conducting kernel principal component analysis on the eigenvector matrix, Table 1 displays the contribution rate and cumulative contribution rate of certain features.

Table 1. Eigenvalues and cumulative variance contribution rates.

Principal Component	Variance Contribution Rate (%)	Cumulative Variance Contribution Rate (%)
power spectrum entropy	66.10	66.10
approximation entropy	12.75	78.85
variance	8.48	87.33
root mean square	6.37	93.70
peak factor	2.71	96.41
sample entropy	1.63	98.04
energy entropy	0.63	98.67
cliff	0.41	99.08

Take the cumulative variance contribution rate as no less than 99%. If the cumulative variance of the first eight principal components in the KPCA results has already reached 99%, then the use of these principal components can achieve dimensionality reduction while retaining most of the data information. Choosing eight principal components is a reasonable solution; it is not too many (avoiding unnecessary computation and complexity) and not too few (avoiding the loss of too much information). Based on the data in Table 1, it is evident that the cumulative contribution rate of the initial eight principal components has exceeded 99.08%. Hence, these eight principal components are chosen to construct a new feature vector that captures the essence of the original data.

4.2. Comparative Analysis and Validation of Experiments

The GIS isolation switch fault-diagnosis simulation can be achieved by utilizing the KPCA algorithm to reduce the dimension of the GIS isolation switch, allowing the low-dimensional feature dataset of various states to be fed into the SVDD algorithm classifier. A Bayesian optimization method is adopted to obtain the optimal penalty constants. Define the search space for two penalty constants as [0.1, 10], select the surrogate model as the Gaussian Process and the acquisition function as the Expected Improvement, train the model using the training set, and evaluate the performance based on the validation set (8:2), aiming to achieve the highest classification accuracy, determining the optimal penalty constant for positive samples as C_1, which is 3.2, and the optimal penalty constant for negative samples as C_2, which is 1.5. Four hundred samples were taken for each type of vibration signal to create a dataset, with 200 groups allotted for training and 200 groups designated for diagnostic sampling. Different positive and negative sample ratios were selected from the diagnostic sample set to form 4 groups of test sample sets. Each group of test sample sets contains 200 groups of samples. The states in the sample sets belonging to the 4 test groups are displayed in Table 2.

Table 2. Sample set of 4 test groups.

Sample Type	Test 1	Test 2	Test 3	Test 4
Normal operation	160	160	160	160
Operating mechanism stuck	40	0	0	0
Single-phase connecting rod off	0	40	0	20
Two-phase connecting rod off	0	0	40	20

In order to intuitively see the effect of the proposed model on the mechanical fault diagnosis of the isolation switch, the improved SVDD algorithm, the SVDD algorithm, and the traditional SVM algorithm were used to simulate the classifier for their similar datasets. The optimal parameters for both the traditional SVDD algorithm and the SVM algorithm are the parameters set. An index was calculated by averaging the overall accuracy of three classification algorithms across multiple tests using different groups of test datasets. The classification accuracy was determined by the ratio of correctly classified samples in each group to the total number of samples. Table 3 displays the fault-diagnosis outcomes of the proposed method and various classifier methods discussed in this paper.

The improved SVDD algorithm, when utilized as a classifier, demonstrates a significantly higher classification accuracy compared to the SVDD algorithm, the Deep SVDD algorithm, the traditional SVM algorithm, and the SVDD-SVM algorithm when applied to different fault samples of the isolation switch data collection. The computation time is the least, which is close to the traditional SVDD algorithm, as shown in Table 3. The classification accuracy of the single-phase and two-phase connecting rod off-fault types of the isolation switch is about 95%. The classification accuracy of the data sample set with two different fault types at the same time also reached 93%. However, the traditional SVDD algorithm and SVM algorithm identify the known faults in the data sample as non-existent fault types, and the classification accuracy is relatively low. The above data demonstrate that the mechanical fault-diagnosis model for isolation switches, utilizing the enhanced SVDD algorithm proposed in this paper, precisely identifies and categorizes various fault samples.

Table 3. GIS isolation switch fault-diagnosis result.

Classifiers	Test Collections	Normal Sample	Operating Mechanism Stuck	Single-Phase Connecting Rod Off	Two-Phase Connecting Rod Off	Classification Accuracy	Computation Time
Improved SVDD	Test 1	151	37	0	0	94%	1.75 s
	Test 2	153	0	38	0	95.5%	1.73 s
	Test 3	153	0	0	37	95%	1.69 s
	Test 4	154	0	17	15	93%	1.75 s
SVDD	Test 1	147	31	3	0	89%	1.69 s
	Test 2	146	1	32	2	89%	1.72 s
	Test 3	145	0	2	31	88%	1.74 s
	Test 4	147	2	14	13	87%	1.68 s
Deep SVDD	Test 1	150	36	0	0	93%	2.25 s
	Test 2	151	0	37	0	94%	2.42 s
	Test 3	149	0	0	36	92.5%	2.13 s
	Test 4	148	0	15	16	89.5%	2.31 s
SVM	Test 1	140	28	2	0	84%	2.10 s
	Test 2	139	3	26	0	82.5%	2.25 s
	Test 3	138	0	3	25	81.5%	2.12 s
	Test 4	140	3	13	12	82.5%	2.31 s
SVDD-SVM	Test 1	150	37	0	0	93.5%	2.75 s
	Test 2	152	0	35	0	93.5%	2.59 s
	Test 3	151	0	0	37	94%	2.62 s
	Test 4	153	0	15	16	92%	2.78 s

5. Conclusions

This paper collects vibration signal data to simulate three typical fault conditions of the isolation switch in GIS, such as the operating mechanism being stuck, the single-phase connecting rod falling off, and the two-phase connecting rod falling off, along with the normal operational state. Firstly, based on information entropy theory, signal features are extracted to obtain multi-dimensional feature data, including entropy values and time-domain features. Furthermore, the KPCA algorithm is applied to lessen the dimensionality of the high-dimensional feature dataset of the isolation switch, resulting in a low-dimensional feature set that exhibits clear differentiation. Finally, a mechanical fault-diagnosis model of the isolation switch based on an improved SVDD algorithm is proposed, and the method is compared with other fault-diagnosis methods. The results demonstrate that this method can effectively identify and differentiate vibration signals generated by the isolation switch in GIS under different operational states. The proposed improved SVDD-algorithm-based isolation switch fault-diagnosis method in this paper offers a new solution for GIS isolation switch fault diagnosis, addressing issues of low detection accuracy and efficiency in conventional fault-diagnosis methods when compared to the traditional SVDD and SVM algorithms.

Author Contributions: Conceptualization, N.Z. and T.W.; methodology, N.Z.; software, T.W. and C.L.; validation, T.W., Y.Z. and B.Y.; formal analysis, Y.Z.; investigation, Y.Z.; resources, B.Y.; data curation, X.Y.; writing—original draft preparation, N.Z.; writing—review and editing, B.Y. and C.L.; visualization, X.Y.; supervision, T.W. and S.L. All authors have read and agreed to the published version of the manuscript.

Funding: This research was supported by the Science and Technology Project of State Grid Liaoning Extra High Voltage Company (research on the on-line monitoring and fault-diagnosis technology of high voltage isolation switch based on feature mining and self-evolutionary learning).

Data Availability Statement: The data presented in this study are available on request from the corresponding authors.

Conflicts of Interest: Authors Nan Zhang, Tianchi Wu, Yunpeng Zhang, Bo Yin and Xuebin Yang were employed by State Grid Liaoning Extra High Voltage Company. The remaining authors declare that the research was conducted in the absence of any commercial or financial relationships that could

be construed as a potential conflict of interest. The authors declare that this study received funding from Science and Technology Project of State Grid Liaoning Extra High Voltage Company. The funder was not involved in the study design, collection, analysis, interpretation of data, the writing of this article or the decision to submit it for publication.

References

1. Hou, Z.; Guo, R.; He, C.; Li, J.; Yao, X. Synergistic effect of SF 6/N 2 gas mixtures on surface partial discharge under DC voltage. *IEEE Trans. Dielectr. Electr. Insul.* **2020**, *27*, 692–699. [CrossRef]
2. Toigo, C.; Vu-Cong, T.; Jacquier, F.; Girodet, A. Partial discharge behavior of protrusion on high voltage conductor in GIS/GIL under high voltage direct current: Comparison of SF 6 and SF 6 alternative gases. *IEEE Trans. Dielectr. Electr. Insul.* **2020**, *27*, 140–147. [CrossRef]
3. Jo, H.E.; Wang, G.; Kim, S.J.; Kil, G.S. Comparison of partial discharge characteristics in SF 6 gas under AC and DC. *Trans. Electr. Electron. Mater.* **2015**, *16*, 323–327. [CrossRef]
4. Razi-Kazemi, A.A.; Shariatnasab, M. A new approach on prioritization of the circuit breakers for installation of online monitoring systems. *IEEE Trans. Power Deliv.* **2019**, *34*, 1569–1577. [CrossRef]
5. Aranizadeh, A.; Shahrtash, S.M.; Gholami, A. Prioritizing CBs maintenance and identifying mandatory maintenance at higher priorities. *Int. Trans. Electr. Energy Syst.* **2022**, *2022*, 5008166. [CrossRef]
6. Li, C.; Sánchez, R.-V.; Zurita, G.; Cerrada, M.; Cabrera, D. Fault diagnosis for rotating machinery using vibration measurement deep statistical feature learning. *Sensors* **2016**, *16*, 895. [CrossRef] [PubMed]
7. Janssens, O.; Slavkovikj, V.; Vervisch, B.; Stockman, K.; Loccufier, M.; Verstockt, S.; Van de Walle, R.; Van Hoecke, S. Convolutional neural network based fault detection for rotating machinery. *J. Sound Vib.* **2016**, *377*, 331–345. [CrossRef]
8. Yue, Y.; Lu, S.; Wang, Y.; Zhang, B. A Fault Diagnosis Method of GIS High Voltage Isolation Switch Based on FA-SVM. In Proceedings of the 2023 5th International Conference on Smart Power & Internet Energy Systems, Shenyang, China, 1–4 December 2023; pp. 47–52.
9. Zhang, J.; Zhao, Y.; Liu, H.; Xu, J.; Peng, S.; Wang, L. Research on fault diagnosis method of GIS isolation switch. In Proceedings of the 2024 3rd International Conference on Energy, Power and Electrical Technology, Chengdu, China, 17–19 May 2024; pp. 1507–1510.
10. Xu, H.; Meng, C.; Huang, Q.; Luo, C.; Zhang, J.; Liu, Z. Time-frequency vibration characteristics analysis of disconnectors of GIS equipment with poor contact mechanical defect. In Proceedings of the 2021 IEEE 5th International Conference on Condition Assessment Techniques in Electrical Systems (CATCON), Kozhikode, India, 3–5 December 2021.
11. Meng, X.; Hu, G.; Liu, Z.; Wang, H.; Zhang, G.; Lin, H.; Sadabadi, M.S. Neural Network-Based Impedance Identification and Stability Analysis for Double-Sided Feeding Railway Systems. *IEEE Trans. Transp. Electrif.* **2024**. [CrossRef]
12. Xie, D.; Lin, C.; Deng, Q.; Lin, H.; Cai, C.; Basler, T.; Ge, X. Simple vector calculation and constraint-based fault-tolerant control for a single-phase CHBMC. *IEEE Trans. Power Electron.* **2024**, *40*, 2028–2041. [CrossRef]
13. Liao, X.; Su, X.; Ren, C.; He, L.; Ding, D.; Zhou, D. Research on circulating current characteristics and the vibration mechanism on the GIS enclosure. In Proceedings of the 2019 2nd International Conference on Electrical Materials and Power Equipment (ICEMPE), Guangzhou, China, 7–10 April 2019.
14. Ji, L.; Fu, C.; Sun, W. Soft fault diagnosis of analog circuits based on a ResNet with circuit spectrum map. *IEEE Trans. Circuits Syst. I Regul. Pap.* **2021**, *68*, 2841–2849. [CrossRef]
15. Liu, Z.; Liu, X.; Xie, S.; Wang, J.; Zhou, X. A novel fault diagnosis method for analog circuits based on multi-input deep residual networks with an improved empirical wavelet transform. *Appl. Sci.* **2022**, *12*, 1675. [CrossRef]
16. Rahimnejad, A.; Gil, M.; Abdoos, A.; Gadsden, S.A. A hybrid intelligent busbar protection strategy using hyperbolic S-transforms and ex-treme learning machines. *Eng. Rep.* **2021**, *3*, e12438. [CrossRef]
17. Gil, M.; Abdoos, A.A. Intelligent busbar protection scheme based on combination of support vector machine and S-transform. *IET Gener. Transm. Distrib.* **2017**, *11*, 2056–2064. [CrossRef]
18. Amirsadri, S.; Mousavirad, S.J.; Ebrahimpour-Komleh, H. A Levy flight-based grey wolf optimizer combined with back-propagation algorithm for neural network training. *Neural Comput. Appl.* **2018**, *30*, 3707–3720. [CrossRef]
19. Liu, W.; Hu, M.; Ye, Z.; Tang, Y.; Wang, Z.; Zhang, L.; Wei, M. Feedforward Neural Network Based on Improved Gray Wolf Optimizer. In Proceedings of the 2019 10th IEEE International Conference on Intelligent Data Acquisition and Advanced Computing Systems: Technology and Applications (IDAACS), Metz, France, 18–21 September 2019.

Disclaimer/Publisher's Note: The statements, opinions and data contained in all publications are solely those of the individual author(s) and contributor(s) and not of MDPI and/or the editor(s). MDPI and/or the editor(s) disclaim responsibility for any injury to people or property resulting from any ideas, methods, instructions or products referred to in the content.